PNAS RESEARCH ARTICLE | CELL BIOLOGY

# Substrate stress relaxation regulates neural stem cell fate commitment

Eric Qiao[a], Camille A. Fulmore[b], David V. Schaffer[a,b,c,1], and Sanjay Kumar[a,c,d,1]

Affiliations are included on p. 9.

Edited by Dennis E. Discher, University of Pennsylvania, Philidelphia, PA; received October 12, 2023; accepted May 17, 2024 by Editorial Board Member Rakesh K. Jain

**Adult neural stem cells (NSCs) reside in the dentate gyrus of the hippocampus, and their capacity to generate neurons and glia plays a role in learning and memory. In addition, neurodegenerative diseases are known to be caused by a loss of neurons and glial cells, resulting in a need to better understand stem cell fate commitment processes. We previously showed that NSC fate commitment toward a neuronal or glial lineage is strongly influenced by extracellular matrix stiffness, a property of elastic materials. However, tissues in vivo are not purely elastic and have varying degrees of viscous character. Relatively little is known about how the viscoelastic properties of the substrate impact NSC fate commitment. Here, we introduce a polyacrylamide-based cell culture platform that incorporates mismatched DNA oligonucleotide-based cross-links as well as covalent cross-links. This platform allows for tunable viscous stress relaxation properties via variation in the number of mismatched base pairs. We find that NSCs exhibit increased astrocytic differentiation as the degree of stress relaxation is increased. Furthermore, culturing NSCs on increasingly stress-relaxing substrates impacts cytoskeletal dynamics by decreasing intracellular actin flow rates and stimulating cyclic activation of the mechanosensitive protein RhoA. Additionally, inhibition of motor–clutch model components such as myosin II and focal adhesion kinase partially or completely reverts cells to lineage distributions observed on elastic substrates. Collectively, our results introduce a unique system for controlling matrix stress relaxation properties and offer insight into how NSCs integrate viscoelastic cues to direct fate commitment.**

neural stem cells | neurogenesis | mechanotransduction | viscoelasticity | stress relaxation

## Significance

It is well established that neural stem cell (NSC) fate is strongly influenced by solid-like properties of the extracellular matrix (ECM), such as stiffness. However, brain ECM is viscoelastic, exhibiting both solid-like and fluid-like qualities. Importantly, viscoelastic properties often change in disease states and aging, raising the question of how these properties contribute to both processes. Using a unique two-dimensional viscoelastic culture system, we find that ECM stress relaxation, a fluid-like property, plays a comparable role to stiffness in determining NSC fate commitment. In particular, ECM stress relaxation drives astrocyte differentiation, an effect mediated by dynamic activation of the Rho GTPase RhoA. Our findings highlight the value of incorporating viscoelasticity in culture platforms to control stem cell differentiation.

Extracellular matrix (ECM) mechanical properties affect a wide range of cell behaviors. In particular, ECM elastic properties such as stiffness have been shown to affect cell migration (1–3), adhesion (4, 5), and differentiation (6–8). However, in addition to elasticity, tissues in vivo exhibit a significant degree of viscous character, such that applied stresses are both internally dissipated and stored (9–11). As with stiffness, the viscous nature of the ECM has been shown to influence cell spreading, differentiation, nascent protein deposition, and matrix remodeling (12, 13). Specifically with regard to neuronal maturation, ECM viscoelasticity has been shown to regulate cell behavior both on the transcriptional and protein level, cementing the importance of viscoelasticity as a cell behavior cue in the brain (14–16).

Substrate stress relaxation, a property specific to viscoelastic materials, has attracted great interest as a potentially important regulator of cell behavior. Stress-relaxing materials exhibit a time-dependent decrease in internal stress under applied strain ("relaxation"), reflecting molecular rearrangements within the material that dissipate rather than store the applied strain. Stress relaxation properties of the ECM have been shown to influence stem cell differentiation (17) and cell spreading (18) in a manner dependent on the amplitude and timescale of relaxation.

While stress relaxation properties can powerfully influence cell behavior, the intracellular mechanisms responsible for sensing and transducing these inputs remain incompletely understood. One concept often proposed for the sensing of matrix-based mechanical cues is the motor–clutch (MC) model for force transmission. According to this model, myosin "motors" drive the retrograde flow of actin, which is opposed by the formation of transmembrane focal adhesions ("clutches"), which transmit stresses between the cell and substrate. The mechanical properties of the substrate influence the behavior of cells by altering the velocity of motors, the dynamics of clutch formation, and the amount of intracellular tension generated (19). The MC model was originally proposed by Mitchison and Kirschner (20) in the context of axonal process extension and later applied by Chan and Odde to explain stiffness-dependent filopodial dynamics (19). More

Author contributions: E.Q., D.V.S., and S.K. designed research; E.Q. and C.A.F. performed research; E.Q. analyzed data; and E.Q., D.V.S., and S.K. wrote the paper.

The authors declare no competing interest.

This article is a PNAS Direct Submission. D.E.D. is a guest editor invited by the Editorial Board.



[1]To whom correspondence may be addressed. Email: schaffer@berkeley.edu or skumar@berkeley.edu.

This article contains supporting information online at https://www.pnas.org/lookup/suppl/doi:10.1073/pnas.2317711121/-/DCSupplemental.

Published July 5, 2024.

recently, motor-clutch-based models have been extended to integrate viscous as well as elastic cues (21, 22), demonstrating how viscoelastic parameters like steady-state stiffness and viscosity interact to influence cell behaviors like spreading.

A core concept of the MC model is that stress transmission between cell and matrix is governed by an interplay between motor-imposed contractile forces and molecular-scale affinity of the clutches. An important barrier to progress in understanding how stress relaxation influences cell behavior is the absence of culture systems in which viscous properties can be quantitatively tuned. Many previous studies have employed alginate hydrogels, where viscoelastic properties have been modulated by varying the relative density of covalent to noncovalent (calcium ion-based) cross-links (17). In this system, the noncovalent cross-links may be transiently broken and reformed in response to cell-imposed stress, thereby relaxing those stresses. While this and related platforms continue to yield important mechanistic insights, the calcium needed for the noncovalent cross-linking may have unintended biological effects, particularly in culture models of highly calcium-sensitive tissues such as heart and nerve (23–25). An alternative approach has been to employ interpenetrating or semi-interpenetrating polymer networks wherein viscous properties arise from the entanglement and disentanglement of polymer chains. Drawbacks of these systems, however, include diffusion and loss of polymer chains from the network and heterogeneities in mechanics and ligand presentation due to the use of multiple polymer types (26). Furthermore, viscoelastic properties in both systems are determined entirely empirically and cannot be easily predicted from the affinity of the constituent cross-links or related to the contractile forces that are generated. Other creative dynamic cross-linking systems have been generated, though they face other challenges. Schiff base-cross-linked gels are commonly formulated using materials like chitosan, whose use has historically been limited by poor solubility or mechanical stability under physiological conditions (27, 28). Likewise, hydrazone cross-linking strategies are highly pH sensitive, with previous formulations displaying poor stability past 5 d under cell culture conditions (29). While strides have been made to improve hydrogel stability in both cases, those strategies typically require specialty modification of polymer backbones (30). As a result, easily accessible viscoelastic matrix platforms whose stress relaxation properties may be understood and controlled in terms of cross-link affinity can further benefit the field.

To address this need, we now introduce a viscoelastic culture system in which stress relaxation can be controlled by tuning the affinity of noncovalent cross-links. Specifically, we synthesize polyacrylamide hydrogels cross-linked with complementary, hybridizing DNA oligonucleotides with defined numbers of base-pair mismatches. We show that increasing the number of mismatches increases stress relaxation without changing basal elastic modulus. When we culture naive neural stem cells (NSCs) on these materials, neural differentiation surprisingly falls and astrocyte differentiation increases with greater stress relaxation, which is accompanied by more rapid oscillation of Rho GTPase activation. Optogenetic stimulation of fast RhoA dynamics on non-stress-relaxing substrates similarly suppresses neurogenesis, supporting a causal link between these dynamics and lineage commitment. This link may be interrupted by pharmacologic disruption of motor and focal adhesion proteins, reinforcing the importance of MC components in transducing viscoelastic cues.

## Results

**Polyacrylamide Hydrogels with Tunable Stress Relaxation Properties.** To tune ECM viscoelastic properties, we introduced a dually cross-linked polyacrylamide hydrogel system stabilized by a combination of covalent and noncovalent cross-links. We chose polyacrylamide (PAAm) as a base polymer due to its widespread use in the field and in our own work to demonstrate the stiffness-sensitivity of NSC lineage commitment (31, 32). However, covalently cross-linked PAAm gels are purely elastic and do not exhibit significant stress relaxation (6, 12). Two common strategies employed to enhance hydrogel viscosity are the introduction of reversible cross-linking chemistries or the entanglement of multiple polymer networks (12, 33). However, entangled polymer networks harbor potential drawbacks. For example, in PAAm/linearized PAAm networks, the linearized network can escape the gel, potentially leading to changes in both mechanical and optical properties over time (34). Meanwhile, interpenetrating networks composed of different polymers often exhibit challenges with ligand stability and presentation as well as heterogenous internal structure when sequential polymerization of the two networks is employed (26).

We therefore introduced a viscoelastic matrix platform in which stress relaxation is induced through reversible DNA oligonucleotide-based cross-links. Previously, we and others had used acrydite-modified oligonucleotides to cross-link PAAm gels to produce time-dependent changes in gel elasticity (35, 36). We hypothesized that we could also build stress relaxation in this system by modifying these cross-links with base-pair mismatches, allowing cross-link rupture and repair under applied strain Fig. 1*A*. To design the location, number, and base pair identity of these mismatches, we designed affinity-tuned mismatched oligonucleotide cross-links with standard, publicly accessible software (37). As we predicted, progressively increasing the number of mismatches from 0 to 4 (henceforth referred to as L0 to L4) increased the degree of stress relaxation Fig. 1*B*. In contrast to ionically cross-linked hydrogels (38), stress did not fall to zero at long timescales in our material. This is consistent with the interpretation that some stress is retained at longer times by the nondynamic bis-acrylamide cross-links. To assess whether the degree of DNA cross-linking changed during cell culture, we measured dsDNA content by SYBR green staining as a function of time in culture and showed both a uniform distribution of DNA cross-links throughout the gels as well as minimal change in DNA content over 6 d Fig. 1*C* and *SI Appendix*, Fig. S1).

To quantify the rate of stress relaxation, we fit our relaxation data to a three-element SLS model of viscoelasticity (Fig. 1*D*), the simplest model of a viscoelastic solid capable of predicting stress relaxation behavior as well as plateauing stress at long times. The stress relaxation behavior of a SLS under constant strain is given by:

$$E(t) = \frac{\sigma(t)}{\varepsilon_{app}} = (E_1 + E_2 e^{\frac{-t}{\tau}}),$$

where $\sigma(t)$ is the time-dependent stress, $\varepsilon_{app}$ is the applied strain, $E_1$ and $E_2$ are the Young's moduli of the spring components, and $\tau$ is the characteristic time scale of relaxation. When we estimated $\tau$ by fitting experimental stress relaxation curves to this model, we found a strong dependence on number of cross-linker mismatches, with $\tau$ ranging from ~175 to ~60 s (Fig. 1*E*). Furthermore, the presence and strength of DNA cross-linkers did not significantly impact the initial elastic modulus of the gels (Fig. 1*F*). Additionally, the ranges for storage, loss, and damping ratio were within range of what has been previously reported in hippocampal tissue (*SI Appendix*, Fig. S2). Finally, changing the amount of DNA incorporated into the gels altered both the degree and rate of relaxation of polyacrylamide gels (*SI Appendix*, Fig. S3*A*).

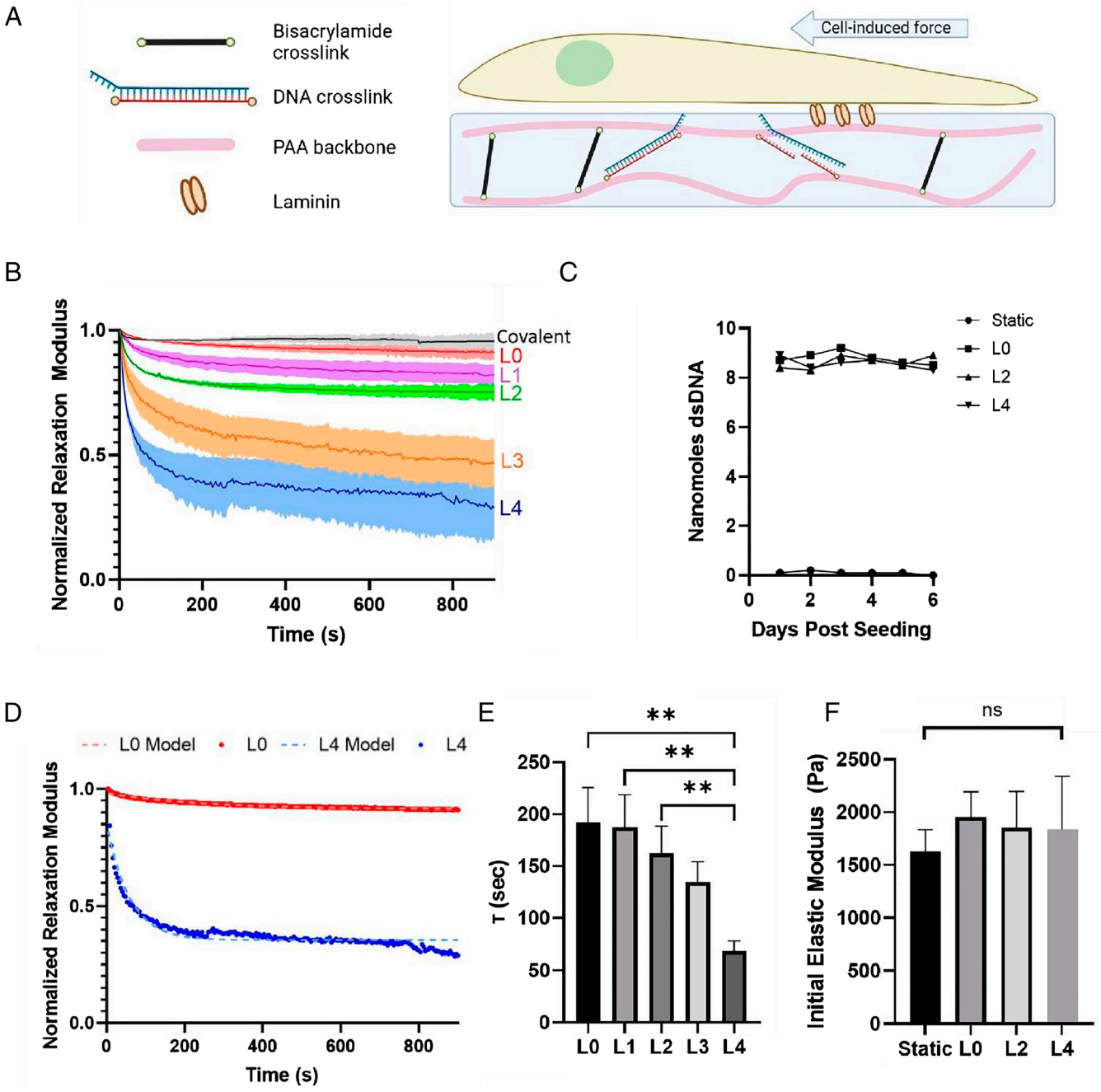


**Fig. 1.** Mismatched DNA cross-linkers enable polyacrylamide hydrogels with tunable stress relaxation properties. (*A*) Schematic representation of dual cross-linking of polyacrylamide hydrogels. DNA-based noncovalent cross-link with two base pair mismatches shown in *Inset*. (*B*) Stress relaxation behavior of gel conditions from (*B*) under constant step strain (10%). Values for relaxation modulus normalized to initial values. (*C*) Stress relaxation data fit to a three-element standard linear solid (SLS) model. The characteristic relaxation time, $\tau$, varies with degree of DNA mismatch. (*D*) Timescales of relaxation in L0 to L4 DNA gels from model fitting. $^{**}P < 0.01$ (one-way ANOVA and Tukey post hoc test). (*E*) Initial elastic modulus measurements of static (DNA-free) and DNA gels containing varying numbers of mismatches (L0 to L4). Measurements performed by shear rheology. No statistical differences in elastic modulus were observed ($P > 0.05$, one-way ANOVA). N = 5 to 7 gels (*F*) DNA content of gels measured by SYBR green staining up to 6 d in culture conditions. Created with BioRender.com.

**Impact of Stress Relaxation on NSC Fate Commitment.** Having established a platform tunable in both degree and rate of stress relaxation, we next investigated the impact of these properties on NSC differentiation. Either rat (Fig. 2 *A* and *B*) or mouse (Fig. 2*C*) NSCs were seeded on 2D gels with varying degrees of stress relaxation and cultured for 7 d under mixed differentiation conditions. Cell fate was then determined by immunostaining for early neuronal marker βIII-tubulin (Tuj1) and astrocytic marker glial fibrillary acidic protein (GFAP) (Fig. 2*A*). Neurogenesis fell significantly on L2 and L4 stress relaxing conditions relative to both the DNA-free static condition and the perfectly base-pair matched L0 condition (Fig. 2 *B* and *C*). The reduction in neurogenesis was comparable to that seen between elastic soft gels with low elastic modulus (~1.5 kPa) and elastic stiff gels (~73 kPa). Conversely, the level of astrogenesis was significantly increased under stress-relaxing conditions relative to static conditions. Again, the magnitude of increase in astrogenesis was comparable to that of soft versus stiff gel conditions with minimal stress relaxation. Furthermore, the progressive increase in these effects from L0 to L2 to L4 suggests that the impact of neurogenesis depends on the degree of substrate stress relaxation.

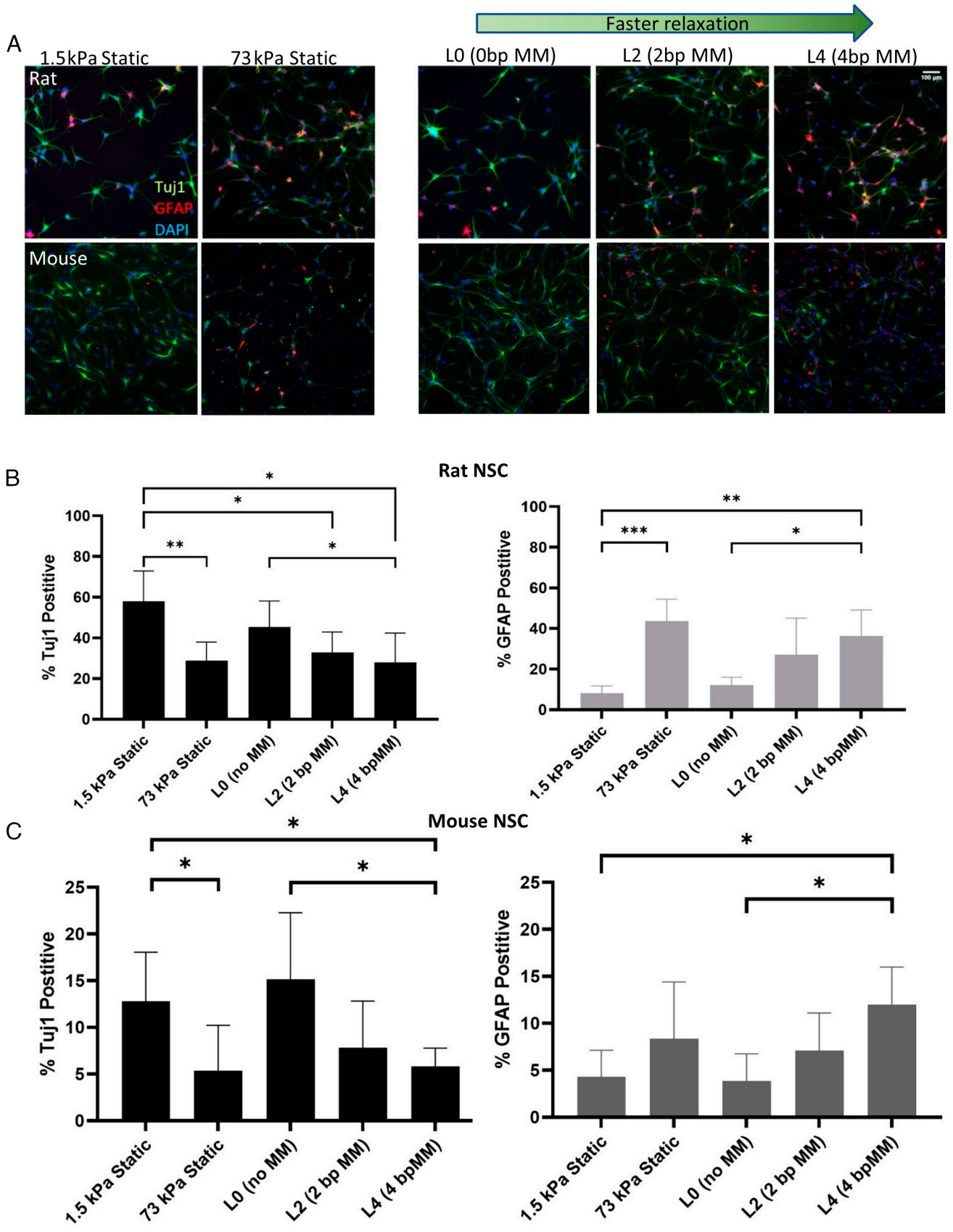


**Fig. 2.** Stress relaxing materials suppress neurogenesis and biases NSCs toward astrocytic fates. (*A*) Representative images of marker signal for neurogenesis, Tuj1 (green) and astrogenesis, GFAP (red) in rat NSCs cultured on soft (1.5 kPa), stiff (73 kPa), and stress relaxing conditions. (Scale bar, 100 µm.) (*B* and *C*) Quantification of fate commitment in rat NSCs (*B*) and mouse NSCs (*C*) on gel conditions from *A*. Quantification performed 6 d after induction of differentiation using mixed differentiation media conditions (1 µM retinoic acid + 1% FBS for rat, 1 µM retinoic acid + FGF withdrawal for mouse). In both rat and mouse NSCs, the proportion of neurons decreases significantly while the proportion of astrocytes increases significantly as the degree of substrate relaxation increases. Error bars represent one SD. $^{*}P < 0.05$, $^{**}P < 0.01$, $^{***}P < 0.001$ (one-way ANOVA and Tukey post hoc test). N = 4 to 6 biological replicates, 450 to 550 cells total.

**MC Model Components Influence Stress Relaxation-Mediated Differentiation.** Having seen that stress relaxation cues significantly influence NSC fate commitment, we next investigated the underlying mechanisms by which cells sense such cues. We chose our targets based on the MC model, where an interplay between actomyosin motor-driven contractility and molecular clutches (e.g., focal adhesions) dictate the degree to which contractile forces are transmitted to the ECM (19). ECM viscoelastic properties are expected to directly and indirectly influence both the motors and clutches. For example, matrix elasticity is predicted to control the rate at which the clutches are mechanically loaded, with force transmission determined by the timescale of loading and the number and lifetimes of available clutches. Successful force transmission impacts intracellular force transmission and downstream mechanotransduction events, such as translocation of Yes-associated protein (YAP) (21, 39).

A key cellular behavior predicted by the motor clutch model is cell spreading (21), so we examined spreading, morphology, and actin flow rates on our stress-relaxing materials. NSCs cultured on stress-relaxing conditions for 24 h spread to larger areas than on nonrelaxing static or L0 gels, with NSC circularity falling on L4 materials (*SI Appendix*, Fig. S4). According to the MC model, increased cell spreading on viscoelastic substrates occurs when increased focal adhesion lifetimes are coupled with restriction of F-actin retrograde flow (21). To test whether these conditions are met in our system, we measured F-actin flow rates in NSCs via confocal fluorescence microscopy with a cell-permeable F-actin probe (Fig. 3*A*) and subjected the resulting videos to particle image velocimetry (PIV) to extract actin flow rates (Fig. 3*B*). NSCs cultured on stress-relaxing substrates had decreased average actin flow rates compared to NSCs cultured on static conditions (Fig. 3 *C* and *D*).

We were also interested to examine the impact of substrate stress relaxation on levels of clutch formation. We stained NSCs for phosphorylated focal adhesion kinase (pFAK), as an indicator for stably engaged clutches with active integrin signaling (Fig. 4*A*) and observed an increase in both the average number of pFAK clusters per cell as well as an increase in the density of clusters normalized by cell area (Fig. 4*B*). Additionally, we examined the activity of RhoA, a Rho-family GTPase that has previously been implicated as a regulator of both NSC fate commitment and adhesion formation (32), (40). G-LISA measurements revealed greater active, GTP-bound RhoA in NSCs cultured on stress-relaxing substrates than non-stress-relaxing substrates (Fig. 4*C*).

Next, we examined whether these motor clutch components exerted a functional role in NSC fate commitment. We used small molecule inhibitors of myosin II (1 μM Blebbistatin) and pFAK (0.5 μM PF-573228) to target activation of the motor (myosin) and clutch (FAK) portions of the model. We observed a decrease in astrocyte differentiation upon treatment with both inhibitors on stress-relaxing substrates, down to a level comparable to static substrate conditions (Fig. 4 *D* and *E*), indicating that both actomyosin contractility and focal adhesion signaling play crucial roles in viscoelastic NSC fate commitment.

**Stress-Relaxing Substrate Regulates Fate Commitment by Cyclic Activation of RhoA.** Given the observed changes in RhoA activation, the known role of RhoA in regulating fate commitment and actomyosin contractility, the time-dependent properties of our hydrogels, and our recent observations that RhoA activity exhibits stiffness-dependent temporal fluctuations that modulate NSC fate (41), we next probed the dynamics of RhoA activity on stress-relaxing substrates. While overall RhoA activation is known to play a role in cell behaviors including spreading, differentiation, and migration (42–44), the temporal dynamics of RhoA activation are also known to play an important role in many of these processes (41, 45–47).

We observed higher overall activation of RhoA on stress-relaxing substrates, and to investigate whether stress relaxation impacts also impacts dynamic RhoA activation, we used a previously

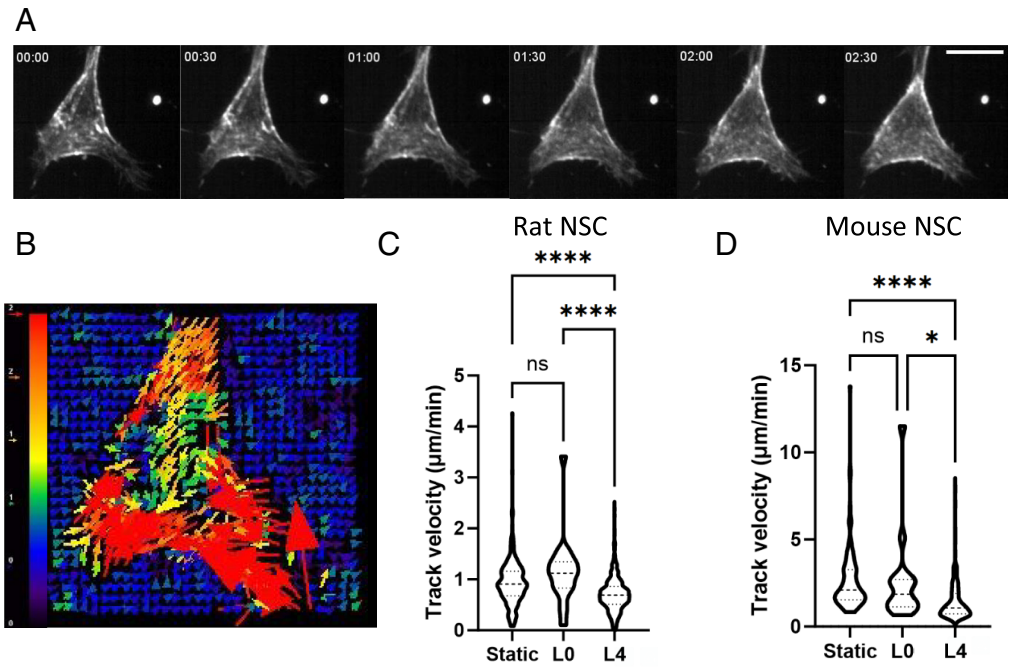


**Fig. 3.** NSCs show reduced actin flow rates on stress relaxing substrates. (*A*) Representative time lapse images of a single mouse NSC with F-actin signal visualized via SiR-Actin live cell fluorescent probe. Full dataset acquired over 15 min per cell. (Scale bar, 10 μm.) (*B*) Actin flow velocity vector plots generated from time-lapse data on static and L4 gels using ImageJ PIV plugin. Velocities interrogated over 10 frames (approx. 40 s). (*C* and *D*) Quantification of actin flow velocities in rat and mouse NSCs. Average actin velocities were obtained by averaging all vector magnitudes generated from vector plots in *B*. In both cell lines, average actin flow velocities were significantly decreased on the stress-relaxing condition. ****$P < 0.0001$ (Mann–Whitney U-test). N = 121 to 156 single cells

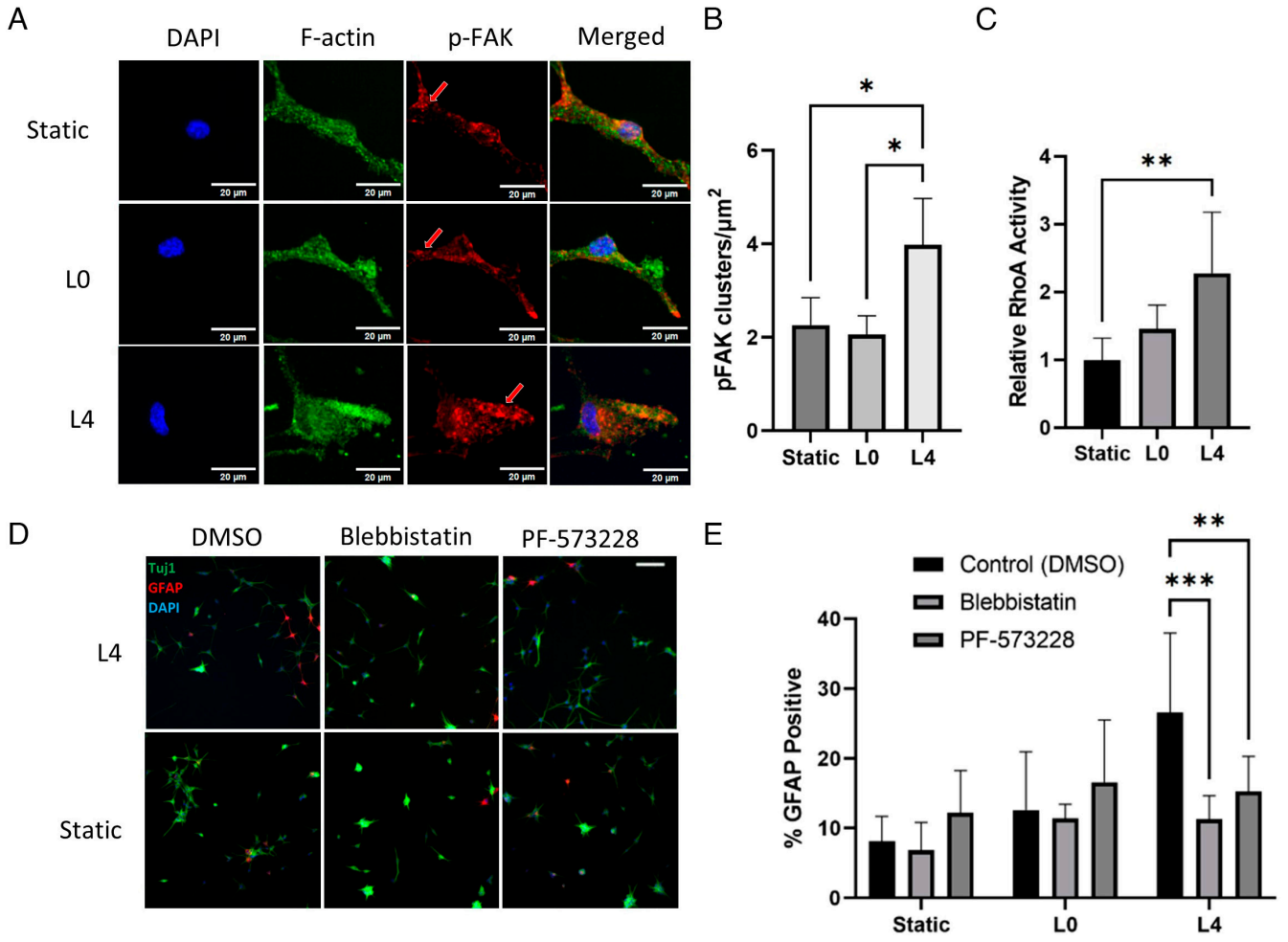


**Fig. 4.** Stress-relaxing substrates promote FAK phosphorylation. (*A*) Representative images of rat NSCs stained with DAPI (blue), F-actin (green), and pFAK (red) after 24 h of differentiation on static or stress relaxing substrates. Arrows denote clustered pFAK signal. (*B*) Quantification of number of pFAK clusters within cells from conditions in *A*. Cluster number was normalized to DAPI count. $*P < 0.05$ (Student's *t* test). (*C*) Relative RhoA activity measured by GLISA for rat, mouse NSCs on stress relaxing substrates after 24 h of differentiation. RhoA activity was significantly increased only on stress relaxing DNA gels. $**P > 0.01$ (one-way ANOVA). (*D*) Representative images of rat NSCs differentiated under myosin II inhibition (blebbistatin) or pFAK inhibition (PF-573228). (Scale bar, 120 μm). (*E*) Quantification of fate commitment in rat NSCs with inhibitor conditions from *D*. $**P < 0.01$, $***P < 0.001$ (one-way ANOVA and Tukey post hoc test). N = 3 to 5 biological replicates, 250 to 350 cells total.

described, genetically encoded FRET-based RhoA biosensor (41, 48) in which a rhotekin-derived Rho-binding domain (RBD) is flanked by a donor and acceptor fluorophore. Upon activation of RhoA, the RBD binds to RhoA-GTP, causing a conformational change in the sensor that brings the donor and acceptor fluorophores together to increase FRET efficiency. Using these biosensors with a ratiometric FRET analysis approach as previously described (41), we observed that the FRET intensity fluctuates over time in NSCs cultured on multiple substrate conditions (Fig. 5 *A* and *C*). Moreover, we observed an oscillation in RhoA activity that was significantly faster in NSCs on stress-relaxing substrates (average peak-to-peak period of ~5 min) compared to NSCs on static substrates (average peak-to-peak period of ~17 min).

These results are consistent with previous reports that external stimuli can cause RhoGTPase activation to fluctuate in a manner that modulates dynamic cell behaviors, including migration and differentiation (41, 49, 50). The timescales of these RhoA pulses were comparable to the previously reported values in studies of migration and protrusion formation (49), however, less has been reported regarding the role of cyclic RhoA activation in regulating stem cell fate commitment. To determine whether cyclic RhoA activation is responsible for the proastrocytic differentiation observed above on stress relaxing substrates, we utilized an NSC line expressing our previously developed light activatable RhoA-Cry2 fusion protein (optoRhoA) (51). Under blue light stimulation, RhoA-Cry2 proteins cluster and drive activation of the RhoA portion of the construct, and by applying pulsatile blue light stimulation, we can strictly control the dynamics of RhoA activation. To examine whether pulsed RhoA activation could influence fate commitment, we cultured NSCs under three illumination conditions: a dark condition, constant illumination (0.5 μW/mm$^2$, "on"), and pulsed illumination with a period of 5 min to mimic the observed frequency from FRET studies but with an overall light dosage equivalent to constant illumination (1 μW/mm$^2$, 50% duty cycle, "on/off"). Similar to naive cells cultured on stress-relaxing substrates, we observed that optoRhoA NSCs cultured on static substrates exhibited greater suppression of neurogenesis and increase in astrogenesis under the on/off illumination condition compared to no or constant illumination (Fig. 5*E*). This result suggests that the pulsed activation of RhoA, at the frequency observed in cells cultured on stress relaxing conditions, is sufficient to induce a similar differentiation phenotype, even on static substrates. Together, these results suggest that substrate stress relaxation contributes to dynamic activation of RhoA and subsequent astrogenesis.

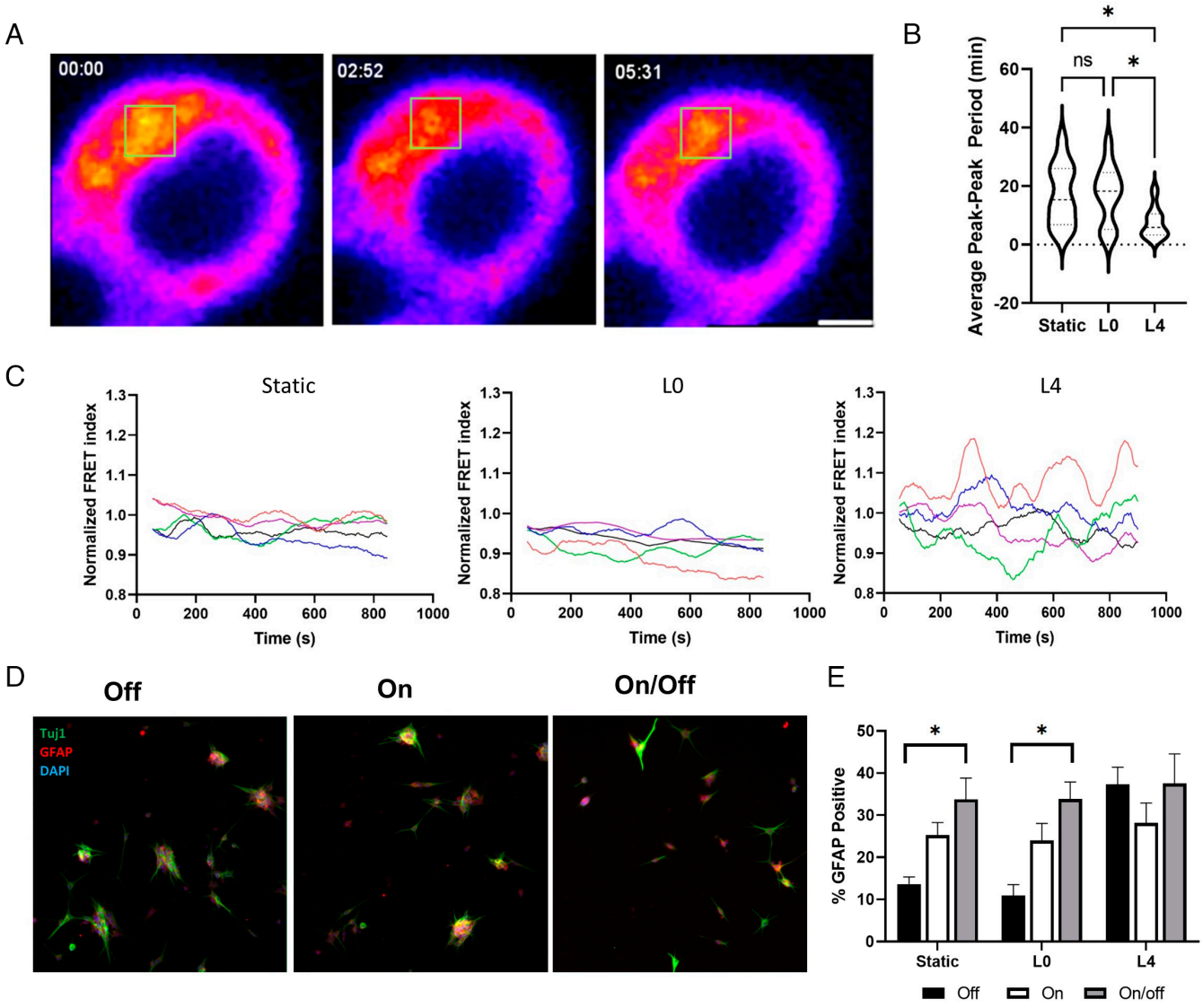


**Fig. 5.** Stress-relaxing substrates promote astrogenesis through cyclical RhoA activation. (*A*) Representative time lapse images of rat NSCs on L4 gels expressing RhoA FRET biosensors (RhoA2g). Intensities indicate value of FRET index as measured by the sensitized emission of fluorescence method. (Scale bar, 5 μm.) (*B*) Distribution of RhoA activation periods as measured by a peak–peak intensities. RhoA activation displays oscillatory behavior with shorter periods on stress relaxing gels when compared to static conditions. N = 10 to 15 individual cells. (*C*) Representative traces of normalized FRET index over 900 s on conditions from (*B*). Each trace represents averaged FRET index over an entire single cell. (*D*) Representative images of rat optoRhoA NSCs differentiated under dark (off), constant illumination (on), and pulsing illumination (on/off) on static gels. (Scale bar, 100 μm). (*E*) Quantification of astrogenesis from conditions in *D* across static, L0, L4 gel conditions. **P* < 0.05 (one-way ANOVA and Tukey post hoc test). N = 3 biological replicates, 300 to 350 cells total.

## Discussion

To investigate the impact of stiffness-independent stress relaxation on NSC lineage commitment, we have developed a dual-cross-linked hydrogel system for NSC culture with tunable viscoelastic properties. Our mismatched oligonucleotide-based cross-linking strategy allowed us to vary stress relaxation without significantly impacting initial elastic modulus (Fig. 1). This method provides a relatively straightforward way to design viscoelastic properties into hydrogel systems. By linearly relating computationally-derived free energies to stress relaxation times, one can design cross-linkers to reach a desired degree of stress relaxation (*SI Appendix*, Fig. S7). The use of DNA cross-linking also offers other benefits over previous noncovalent cross-linking strategies, as we can modulate strength of cross-linking based on sequence, cross-linker length, and cross-linker density, thereby offering significant degrees of freedom beyond cross-linker density and polymer molecular weight. While the loss modulus of L4 gels is higher (*SI Appendix*, Fig. S2), there is still a nonzero loss modulus in static and L0 gels, suggesting some viscous character even in baseline polyacrylamide gels. However, this observation does not seem to translate into significant stress relaxation, perhaps owing to the difference in testing modalities (oscillatory vs nonoscillatory). We next investigated the impact of stress relaxation on NSC behavior and found that such relaxation significantly impacts differentiation by suppressing neurogenesis and increasing astrogenesis (Fig. 2), analogous to our past reports on stiffer elastic substrates (32, 52). Previously, it had been shown that NSCs switched from a stiff to soft substrate exhibited higher neurogenesis (36). As we see the opposite effect in stress-relaxing gels, our results are consistent with the idea that cellular responses to stress relaxation induced by reversible noncovalent cross-links cannot simply be thought of as analogous to softening of an elastic material.

Previous studies have shown that the MC model of force transmission may play an important role in the transduction of viscoelastic cues. In particular, Gong et al. predicted that cellular

response to such cues is dependent on the relative values of several timescales: the timescale of substrate relaxation ($\tau_s$), timescale of clutch binding ($\tau_b$), and timescale of clutch lifetime ($\tau_l$), with maximal cell spreading when $\tau_b < \tau_s < \tau_l$ (21). The authors noted that when $\tau_s < \tau_b$, the substrate relaxes faster than clutches are binding to the substrate, meaning cells only experience a fully relaxed, low stiffness that fails to impede actin retrograde flow and leads to lower cell spreading. Conversely, when $\tau_s > \tau_l$, the force on clutches does not diminish due to relaxation over the clutch lifetime, causing clutches to load and fail prematurely and reducing impairment of retrograde flow, also leading to lower overall spreading. When $\tau_b < \tau_s < \tau_l$, clutches do not fail prematurely due to lack of relaxation while still presenting a relatively high effective substrate stiffness to slow retrograde flow. Given reported clutch binding timescales of ~1 s and focal adhesion lifetimes on the order of tens of minutes (53), it seems likely that our system ($\tau_s$ = 60 s for L4) would fall within this regime of high focal adhesion lifetime and cell spreading. Our measurements of cell area and actin flow rates are consistent with this prediction, showing larger cell areas (*SI Appendix*, Fig. S4) and lower actin flow rates (Fig. 3 *C* and *D*), as well as an overall higher amount of pFAK clustering on stress relaxing substrates (Fig. 4 *A* and *B*). In comparing the impact of viscoelasticity on pFAK clustering as well as the effects of motor clutch inhibition on NSC differentiation, we find that viscoelasticity generally produces pFAK clustering results similar to that of stiff hydrogels (*SI Appendix*, Figs. S5 and S6). Of note, a consequence of the above relationship between $\tau_b$, $\tau_s$, and $\tau_l$ suggests that a further increase in stress relaxation may eventually reverse the enhanced astrogenesis phenotype described here. An important area for future studies would be to characterize MC parameters more thoroughly on substrates with even more pronounced stress relaxation properties to verify the applicability of this model to NSC differentiation.

While the impacts of viscoelasticity and the clutch model are relatively well studied in the context of cell spreading, their role in NSC differentiation had not been studied. We previously identified the Rho GTPase RhoA as a key regulator of mechanosensitive astrocyte differentiation in NSCs. Although we expected an overall increase in RhoA activity on stress-relaxing substrates, we also observed a cyclic activation of RhoA that occurred at higher frequencies in cells cultured on stress-relaxing substrates compared to those on static substrates (Fig. 5*B*). While previous studies had implicated cycles of matrix strain and relaxation to be key in driving long-term integrin clustering (17), to our knowledge, it has not been shown that matrix stress relaxation directly drives cyclic RhoA activation at time scales comparable to material relaxation timescales to influence fate commitment. Additionally, we observed that protrusion extension and retraction were faster in undifferentiated NSCs cultured on stress-relaxing substrates (*SI Appendix*, Fig. S8). At the same time, we observed that pulsed optogenetic activation of RhoA at a similar frequency is sufficient to drive a comparable fate commitment phenotype as on nonrelaxing substrates (Fig. 5 *D* and *E*). Pulsatile dynamics are frequently encountered in the regulation of genetic circuits and play a role in regulating coordinated gene expression (54). In NSCs, this type of behavior has been shown to play important roles in the context of fate commitment where pulsatile and sustained expression of the same gene can cause different fate commitment phenotypes (55).

The molecular mechanism by which stress-relaxing substrates alter the frequency of RhoA activation is likewise not currently understood. In general, cells that exhibit pulsatile RhoA activity do so with one of two patterns: focal pulses, in which pulse frequency is variable and there is no spatial propagation of pulses, and oscillatory waves that are more regular in frequency and propagate across a cell (56). The patterns of RhoA activity observed in NSCs more closely resemble focal pulses due to the variable frequency and localized presentation (*SI Appendix*, Fig. S9). The mechanisms of RhoA focal pulse generation are often found to be the result of changes in actin dynamics involving downstream effectors of RhoA itself, such as formins and myosins (56, 57). According to these studies, a reduction in actin polymerization rates through depletion of formins was found to induce RhoA focal pulses while similar contractile pulses require the activity of myosin IIA isoform. This is consistent with our results demonstrating the coupling of localized RhoA pulses, reduced actin flow rates, and the requirement of myosin II for stress relaxation–induced astrogenesis. We note that stiff substrates also tend to increase oscillatory RhoA activation (*SI Appendix*, Fig. S11), suggesting that RhoA oscillations play a role in both stiffness and stress relaxation sensing. However, further study is needed to fully confirm the applicability of these pathways to NSCs as well as to identify possible downstream effectors. Smads, previously identified as acting downstream of mechanosensitive RhoA activation, is one such group of candidate (41). Finally, we note that it seems that RhoA fluctuations do not seem to account for both suppression of neurogenesis and increase in astrogenesis, making more detailed optoRhoA experiments necessary in future experiments to further refine RhoA's role in viscoelasticity sensing.

In addition to establishing connections between substrate stress relaxation, changes in cytoskeletal dynamics, and enhanced astrogenesis (Fig. 6), we developed a hydrogel cross-linking strategy that can be readily applied in the design of other biomaterials. However, there are currently limitations on the achievable mechanical properties of this system, such as the fact that we have effectively maximized the achievable stress relaxation using this current gel formulation. Additional optimization to further improve stress relaxation in a wider variety of initial stiffnesses would be valuable for future studies. Although this study sheds light on how stress relaxation in isolation influences NSC differentiation, additional experiments would be necessary to fully elucidate how multiple mechanical properties combine to inform cell behavior. For example, the stiffness of hippocampal tissue (50 to 200 Pa) (58) has been reported to be softer than the initial stiffness conditions investigated here, raising the interesting question of how these results might change on even softer substrates. Extending our materials to ~0.1 kPa stiffness values will require addressing several challenges inherent to such soft hydrogels, including management of swelling, creation of a flat, wrinkle-free culture interface, and obtaining clean, reproducible rheological measurements. Furthermore, given the toxicity of monomeric PAA, this system is not suitable for 3D cell culture and would require optimization to work with a different polymer backbone. Nonetheless, the variety of chemical modifications available for oligonucleotide modification gives DNA cross-linking broad applicability across different materials, as in theory, any material that can incorporate chemically modified DNA could be cross-linked in this manner.

## Materials and Methods

**Polyacrylamide Gel Formation.** Polyacrylamide (PAAm) gels were formed by free-radical initiated, vinyl addition polymerization between monomeric polyacrylamide (Bio-Rad) and N, N′-methylene-bis-acrylamide (bis-acrylamide; Bio-Rad) using a protocol similar to that described previously (32). To summarize briefly, monomeric polyacrylamide and bis-acrylamide precursor solution was mixed at varying molar ratios depending on the desired initial stiffness. Polymerization of gels was then initiated by the addition of ammonium persulfate (APS; Bio-Rad) and tetramethylethylenediamine (TEMED; Bio-Rad). Before complete polymerization, acrylamide precursor solution was sandwiched

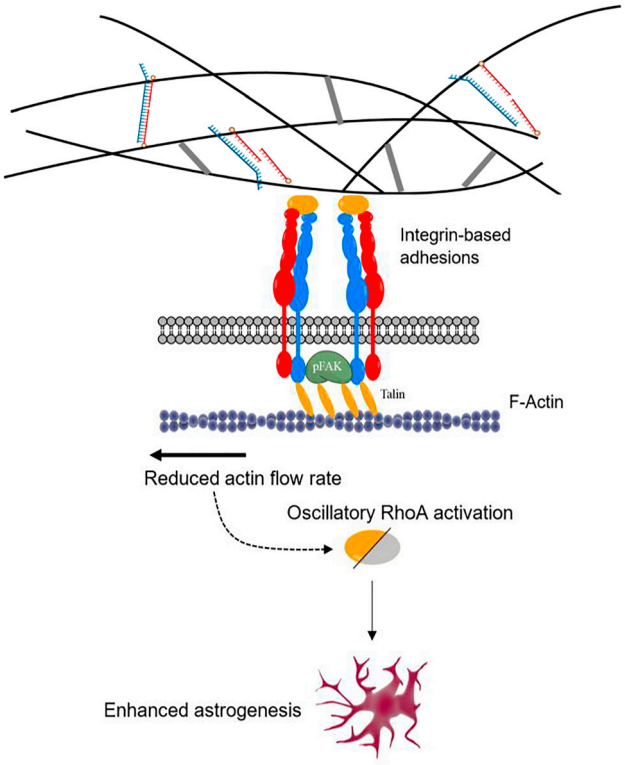


**Fig. 6.** Proposed pathway components for enhanced astrogenesis of NSCs on stress-relaxing substrates. Stress relaxation induces the formation of greater numbers of pFAK-positive clutches, leading to reduced actin flow rates. Oscillatory RhoA is observed with reduced actin flow rates, though a direct connection is not yet shown. High-frequency oscillatory RhoA activity is sufficient to drive increased astrogenesis. Created with BioRender.com.

between a hydrophobic glass surface and a Bind-Silane-treated glass coverslip (GE Healthcare). PAAm gels were further modified with DNA oligos to induce viscoelastic properties. Acrydite-functionalized DNA side arms (IDT) were allowed to hybridize with unmodified linkers at equimolar concentrations for 20 min at room temperature. Hybridized DNA complexes were then mixed into the polyacrylamide/bis-acrylamide precursor solution for 20 min at room temperature. The final DNA concentration in viscoelastic gels is 150 μM. Polymerization then proceeds as described above. For cell work, all PAAm gels were surface functionalized with laminin after polymerization, as previously described (31). Briefly, 25 μg/mL (50 μg/mL for mouse NSCs) mouse laminin was conjugated to the gel surface via UV light-initiated sulfosuccinimidyl 6-(4′-azido-2′-nitrophenylamino) hexanoate (sulfo-SANPAH; Thermo-Fisher) chemistry.

**Rheological Characterization of Polyacrylamide Gels.** All rheological measurements were carried out on an MCR 301 rheometer (Anton-Paar) using a parallel plate geometry (20 mm diameter). All measurements were carried out at 37 °C in a humidified chamber to prevent drying out of the gels. Then, ~200-μm-thick gels were formed directly on the rheometer stage according to the protocol described above. For stress relaxation measurements, a constant 10% strain was applied over 15 min. For initial elastic modulus measurements, oscillatory strain was applied with an amplitude of 0.5% and a frequency of 1 Hz.

**NSC Culture and Differentiation.** Rat hippocampal NSCs were isolated from adult female Fischer 344 rats as described previously (59) and were cultured in DMEM/F12 supplemented with N2 (Thermo-Fisher). Media were supplemented with 20 ng/mL of FGF (Peprotech) in proliferation conditions and with 1% FBS + 1 μM retinoic acid (Sigma-Aldrich) in mixed differentiation conditions. Mouse hippocampal NSCs were isolated from adult C57BL6/J mice as described previously (60) and were cultured in Neurobasal-A media supplemented with B27 without Vitamin A and Glutamax supplement (Thermo-Fisher). Media was additionally supplemented with 20 ng/mL each of FGF and EGF (Peprotech) for proliferation conditions. To achieve mixed differentiation conditions, mouse NSCs were cultured in Neurobasal-A with 1 μM retinoic acid and gradual FGF withdrawal (20 ng/mL for 24 h, 10 ng/mL for 48 h, 1 ng/mL beyond 48 h). Cells seeded on gels were seeded at a density of 25,000 cells/μm$^2$. All differentiation assays were performed at the end of a 7 d culture period. Cell morphology and actin flow rate studies were performed 48 h after cell seeding.

**Cell Fixation and Immunocytochemistry.** Cells were fixed with 4% paraformaldehyde (PFA; Alfa Aesar) for 15 min and then washed with phosphate-buffered saline (PBS). Cells were then permeabilized in 0.5% Triton X-100 (Sigma-Aldrich) + 5% donkey serum (Sigma-Aldrich) for 15 min followed by blocking in 5% donkey serum for 1 h. Primary antibody staining was performed overnight at 4 °C at 1:500 for Tuj1 (Sigma Aldrich, Catalog# T5201), 1:1,000 for GFAP (Abcam, Catalog# ab7260), and 1:500 for pFAK (Abcam, Catalog# ab81298). Secondary staining was performed for 2 h at room temperature. Primary and secondary antibodies were diluted in PBS + 5% donkey serum.

**Actin Flow Rate Measurements.** Live NSCs were seeded on gels at 10,000 cells/cm$^2$ and were stained with 100 nM fluorescent SiR-actin probes (Cytoskeleton, Inc.) for 6 h. Imaging was performed at 37 °C with 5% $CO_2$.

**Measurement of Phosphorylated RhoA.** Levels of phosphorylated RhoA were measured using a G-LISA Small G-protein Activation Assay kit (Cytoskeleton, Inc.) according to the manufacturer's protocol. NSCs were lysed directly from gel surfaces, and lysates were stored at −80 °C after clarification and snap-freezing with dry ice. Samples were analyzed by measuring absorbance at 490 nm on a plate reader.

**FRET Measurement of RhoA Activity.** RhoA activity in rat NSCs was measured using FRET-based RhoA biosensors described previously (48). Rat NSCs were stably transduced with constructs encoding the RhoA2g biosensor. Imaging was performed on a ZEISS LSM 880 confocal microscope. Cells were imaged for 900 s at 15-s time points to avoid bleaching. RhoA activity was reported as FRET index as calculated by a sensitized emission method.

**Optogenetic Activation of RhoA.** Rat NSCs were transduced with constructs encoding RhoA-Cry2 fusion protein. Blue light illumination was performed using previously reported LED-based illumination devices (61) using 470 nm blue light. Periodic illumination was applied for the first 48 h of differentiation, after which all conditions were cultured without illumination.

**Data, Materials, and Software Availability.** All study data are included in the article and/or *SI Appendix*.

**ACKNOWLEDGMENTS.** We kindly thank Mary West (University of California, Berkeley, CA), Denise Schnines (University of California, Berkeley, CA), and Holly Aaron (University of California, Berkeley, CA) for their help in optimizing various imaging and microscopy protocols. This project was supported by the NIH (5R01NS074831 to S.K. and D.V.S.) and by the NIH Stem Cell Biological Engineering Training Program (5T32GM098218 to E.Q.).

Author affiliations: [a]Department of Chemical and Biomolecular Engineering, University of California, Berkeley, CA 94720; [b]Department of Molecular and Cell Biology, University of California, Berkeley, CA 94720; [c]Department of Bioengineering, University of California, Berkeley, CA 94720; and [d]Department of Bioengineering and Therapeutic Sciences, University of California, San Francisco, CA 94143

1. C. M. Lo, H. B. Wang, M. Dembo, Y. L. Wang, Cell movement is guided by the rigidity of the substrate. *Biophys. J.* **79**, 144–152 (2000).
2. L. Trichet *et al.*, Evidence of a large-scale mechanosensing mechanism for cellular adaptation to substrate stiffness. *Proc. Natl. Acad. Sci. U.S.A.* **109**, 6933–6938 (2012).
3. M. Ehrbar *et al.*, Elucidating the role of matrix stiffness in 3D cell migration and remodeling. *Biophys. J.* **100**, 284–293 (2011).
4. G. Giannone *et al.*, Periodic lamellipodial contractions correlate with rearward actin waves. *Cell* **116**, 431–443 (2004).
5. Y.-C. Yeh, J.-Y. Ling, W.-C. Chen, H.-H. Lin, M.-J. Tang, Mechanotransduction of matrix stiffness in regulation of focal adhesion size and number: Reciprocal regulation of caveolin-1 and β1 integrin. *Sci. Rep.* **7**, 15008 (2017).
6. A. J. Engler, S. Sen, H. L. Sweeney, D. E. Discher, Matrix elasticity directs stem cell lineage specification. *Cell* **126**, 677–689 (2006).
7. K. Ye, L. Cao, S. Li, L. Yu, J. Ding, Interplay of matrix stiffness and cell-cell contact in regulating differentiation of stem cells. *ACS Appl. Mater. Interfaces* **8**, 21903–21913 (2016).

8. J. S. Park *et al.*, The effect of matrix stiffness on the differentiation of mesenchymal stem cells in response to TGF-β. *Biomaterials* **32**, 3921–3930 (2011).
9. F. Sauer *et al.*, Collagen networks determine viscoelastic properties of connective tissues yet do not hinder diffusion of the aqueous solvent. *Soft Matter* **15**, 3055–3064 (2019).
10. K. E. Kasza *et al.*, The cell as a material. *Curr. Opin. Cell Biol.* **19**, 101–107 (2007).
11. A. E. Kerdok, M. P. Ottensmeyer, R. D. Howe, Effects of perfusion on the viscoelastic characteristics of liver. *J. Biomech.* **39**, 2221–2231 (2006).
12. E. E. Charrier, K. Pogoda, R. G. Wells, P. A. Janmey, Control of cell morphology and differentiation by substrates with independently tunable elasticity and viscous dissipation. *Nat. Commun.* **9**, 449 (2018).
13. C. Loebel, R. L. Mauck, J. A. Burdick, Local nascent protein deposition and remodelling guide mesenchymal stromal cell mechanosensing and fate in three-dimensional hydrogels. *Nat. Mater.* **18**, 883–891 (2019).
14. J. G. Roth *et al.*, Tunable hydrogel viscoelasticity modulates human neural maturation. *Sci. Adv.* **9**, eadh8313 (2024).
15. C. M. Tringides *et al.*, Tunable conductive hydrogel scaffolds for neural cell differentiation. *Adv. Healthc. Mater.* **12**, 2202221 (2023).
16. M. Darnell *et al.*, Material microenvironmental properties couple to induce distinct transcriptional programs in mammalian stem cells. *Proc. Natl. Acad. Sci. U.S.A.* **115**, E8368–E8377 (2018).
17. O. Chaudhuri *et al.*, Hydrogels with tunable stress relaxation regulate stem cell fate and activity. *Nat. Mater.* **15**, 326–334 (2016).
18. W. Yu *et al.*, Gradual stress-relaxation of hydrogel regulates cell spreading. *Int. J. Mol. Sci.* **23**, 5170 (2022).
19. C. E. Chan, D. J. Odde, Traction dynamics of filopodia on compliant substrates. *Science (1979)* **322**, 1687–1691 (2008).
20. T. Mitchison, M. Kirschner, Cytoskeletal dynamics and nerve growth. *Neuron* **1**, 761–772 (1988).
21. Z. Gong *et al.*, Matching material and cellular timescales maximizes cell spreading on viscoelastic substrates. *Proc. Natl. Acad. Sci. U.S.A.* **115**, E2686–E2695 (2018).
22. M. Bennett *et al.*, Molecular clutch drives cell response to surface viscosity. *Proc. Natl. Acad. Sci. U.S.A.* **115**, 1192–1197 (2018).
23. M. M. Pathak *et al.*, Stretch-activated ion channel Piezo1 directs lineage choice in human neural stem cells. *Proc. Natl. Acad. Sci. U.S.A.* **111**, 16148–16153 (2014).
24. C. Leclerc, M. Moreau, I. Néant, The calcium: An early signal that initiates the formation of the nervous system during embryogenesis. *Front. Mol. Neurosci.* **5**, 3 (2012).
25. F. M. P. Tonelli *et al.*, Stem cells and calcium signaling. *Adv. Exp. Med. Biol.* **740**, 891–916 (2012).
26. X. Tong, F. Yang, Engineering interpenetrating network hydrogels as biomimetic cell niche with independently tunable biochemical and mechanical properties. *Biomaterials* **35**, 1807–1815 (2014).
27. M. Rizwan, A. E. G. Baker, M. S. Shoichet, Designing hydrogels for 3D cell culture using dynamic covalent crosslinking. *Adv. Healthc. Mater.* **10**, 2100234 (2021).
28. K. Thirupathi *et al.*, Update on chitosan-based hydrogels: preparation, characterization, and its antimicrobial and antibiofilm applications. *Gels* **9**, 35 (2023).
29. N. Boehnke, C. Cam, E. Bat, T. Segura, H. D. Maynard, Imine hydrogels with tunable degradability for tissue engineering. *Biomacromolecules* **16**, 2101–2108 (2015).
30. T. Hozumi, T. Kageyama, S. Ohta, J. Fukuda, T. Ito, Injectable hydrogel with slow degradability composed of gelatin and hyaluronic acid cross-linked by Schiff's base formation. *Biomacromolecules* **19**, 288–297 (2018).
31. R. J. Pelham Jr., Y. l Wang, Cell locomotion and focal adhesions are regulated by substrate flexibility. *Proc. Natl. Acad. Sci. U.S.A.* **94**, 13661–13665 (1997).
32. A. J. Keung, E. M. de Juan-Pardo, D. V. Schaffer, S. Kumar, Rho GTPases mediate the mechanosensitive lineage commitment of neural stem cells. *Stem Cells* **29**, 1886–1897 (2011).
33. D. D. McKinnon, D. W. Domaille, J. N. Cha, K. S. Anseth, Biophysically defined and cytocompatible covalently adaptable networks as viscoelastic 3D cell culture systems. *Adv. Mater.* **26**, 865–872 (2014).
34. E. E. Charrier *et al.*, A novel method to make viscoelastic polyacrylamide gels for cell culture and traction force microscopy. *APL Bioeng.* **4**, 36104 (2020).
35. D. C. Lin, B. Yurke, N. A. Langrana, Mechanical properties of a reversible, DNA-crosslinked polyacrylamide hydrogel. *J. Biomech. Eng.* **126**, 104–110 (2004).
36. S. Rammensee, M. S. Kang, K. Georgiou, S. Kumar, D. V. Schaffer, Dynamics of mechanosensitive neural stem cell differentiation. *Stem Cells* **35**, 497–506 (2017).
37. J. N. Zadeh *et al.*, NUPACK: Analysis and design of nucleic acid systems. *J. Comput. Chem.* **32**, 170–173 (2011).
38. F. Charbonier, D. Indana, O. Chaudhuri, Tuning viscoelasticity in alginate hydrogels for 3D cell culture studies. *Curr. Protoc.* **1**, e124 (2021).
39. A. Elosegui-Artola *et al.*, Mechanical regulation of a molecular clutch defines force transmission and transduction in response to matrix rigidity. *Nat. Cell Biol.* **18**, 540–548 (2016).
40. H. Warner, B. J. Wilson, P. T. Caswell, Control of adhesion and protrusion in cell migration by Rho GTPases. *Curr. Opin. Cell Biol.* **56**, 64–70 (2019).
41. R. G. Sampayo, M. Sakamoto, M. Wang, S. Kumar, D. V. Schaffer, Mechanosensitive stem cell fate choice is instructed by dynamic fluctuations in activation of Rho GTPases. *Proc. Natl. Acad. Sci. U.S.A.* **120**, e2219854120 (2023).
42. W. T. Arthur, K. Burridge, RhoA inactivation by p190RhoGAP regulates cell spreading and migration by promoting membrane protrusion and polarity. *Mol. Biol. Cell* **12**, 2711–2720 (2001).
43. J. Xu *et al.*, Divergent signals and cytoskeletal assemblies regulate self-organizing polarity in neutrophils. *Cell* **114**, 201–214 (2003).
44. R. McBeath, D. M. Pirone, C. M. Nelson, K. Bhadriraju, C. S. Chen, Cell Shape, cytoskeletal tension, and RhoA regulate stem cell lineage commitment. *Dev. Cell* **6**, 483–495 (2004).
45. B. D. Khalil *et al.*, The regulation of RhoA at focal adhesions by StarD13 is important for astrocytoma cell motility. *Exp. Cell Res.* **321**, 109–122 (2014).
46. F. M. Vega, G. Fruhwirth, T. Ng, A. J. Ridley, RhoA and RhoC have distinct roles in migration and invasion by acting through different targets. *J. Cell Biol.* **193**, 655–665 (2011).
47. A. B. Jaffe, A. Hall, RHO GTPASES: Biochemistry and biology. *Annu. Rev. Cell Dev. Biol.* **21**, 247–269 (2005).
48. R. D. Fritz *et al.*, A versatile toolkit to produce sensitive FRET biosensors to visualize signaling in time and space. *Sci. Signal.* **6**, rs12 (2013).
49. A. Bolado-Carrancio *et al.*, Periodic propagating waves coordinate RhoGTPase network dynamics at the leading and trailing edges during cell migration. *eLife* **9**, e58165 (2020).
50. S. Charrasse *et al.*, RhoA GTPase regulates M-cadherin activity and myoblast fusion. *Mol. Biol. Cell* **17**, 749–759 (2006).
51. L. J. Bugaj, A. T. Choksi, C. K. Mesuda, R. S. Kane, D. V. Schaffer, Optogenetic protein clustering and signaling activation in mammalian cells. *Nat. Methods* **10**, 249–252 (2013).
52. K. Saha *et al.*, Substrate modulus directs neural stem cell behavior. *Biophys. J.* **95**, 4426–4438 (2008).
53. M. E. Rosen, J. C. Dallon, A mathematical analysis of focal adhesion lifetimes and their effect on cell motility. *Biophys. J.* **121**, 1070–1080 (2022).
54. J. H. Levine, Y. Lin, M. B. Elowitz, Functional roles of pulsing in genetic circuits. *Science (1979)* **342**, 1193–1200 (2013).
55. R. Kageyama, S. Ochi, R. Sueda, H. Shimojo, The significance of gene expression dynamics in neural stem cell regulation. *Proc. Jpn. Acad. Ser. B, Phys. Biol. Sci.* **96**, 351–363 (2020).
56. B. Yao, S. Donoughe, J. Michaux, E. Munro, Modulating RhoA effectors induces transitions to oscillatory and more wavelike RhoA dynamics in *Caenorhabditis elegans* zygotes. *Mol. Biol. Cell* **33**, ar58 (2022).
57. M. A. Baird *et al.*, Local pulsatile contractions are an intrinsic property of the myosin 2A motor in the cortical cytoskeleton of adherent cells. *Mol. Biol. Cell* **28**, 240–251 (2016).
58. T. Luque, M. S. Kang, D. V. Schaffer, S. Kumar, Microelastic mapping of the rat dentate gyrus. *R. Soc. Open Sci.* **3**, 150702 (2016).
59. T. D. Palmer, E. A. Markakis, A. R. Willhoite, F. Safar, F. H. Gage, Fibroblast growth factor-2 activates a latent neurogenic program in neural stem cells from diverse regions of the adult CNS. *J. Neurosci.* **19**, 8487–8497 (1999).
60. H. Babu *et al.*, A protocol for isolation and enriched monolayer cultivation of neural precursor cells from mouse dentate gyrus. *Front. Neurosci.* **5**, 89 (2011).
61. N. A. Repina, H. J. Johnson, T. McClave, R. S. Kane, D. V. Schaffer, Protocol to fabricate engineered illumination devices for optogenetic control of cellular signaling dynamics. *STAR Protoc.* **1**, 100141 (2020).